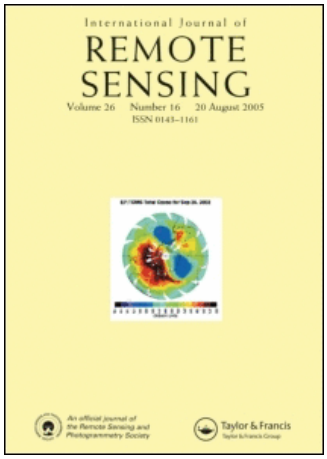

International Journal of Remote Sensing
Publication details, including instructions for authors and subscription information:
http://www.informaworld.com/smpp/title~content=t713722504

Granulometric analyses of basin-wise DEMs: a comparative study

Online Publication Date: 01 January 2007
To cite this Article: Tay, L. T., Sagar, B. S. Daya and Chuah, H. T. (2007) 'Granulometric analyses of basin-wise DEMs: a comparative study', International Journal of Remote Sensing, 28:15, 3363 - 3378
To link to this article: DOI: 10.1080/01431160600981558
URL: http://dx.doi.org/10.1080/01431160600981558

International Journal of Remote Sensing
Vol. 28, No. 15, 10 August 2007, 3363–3378

Granulometric analyses of basin-wise DEMs: a comparative study

L. T. TAY*†, B. S. DAYA SAGAR‡ and H. T. CHUAH†
†Faculty of Engineering, Multimedia University, Cyberjaya Campus, Jalan Multimedia, 63100 Cyberjaya, Selangor, Malaysia
‡Faculty of Engineering and Technology, Melaka Campus, Multimedia University, Jalan Ayer Keroh Lama, 75450, Melaka, Malaysia

(*Received 3 August 2006; in final form 30 August 2006*)

Digital elevation models (DEMs) are very useful for terrain characterization. We apply a morphological approach to characterize 14 sub-basins decomposed from interferometrically generated DEMs of Cameron Highlands and Petaling regions of Peninsular Malaysia. Physiographically, these two regions possess a distinct geomorphologic set-up as they belong to region with higher and lower altitudes, respectively. Fourteen sub-basins are extracted from the DEMs, and pattern spectra by opening and closing of these sub-basins relative to flat discrete binary patterns (square, octagon and rhombus) are computed. Pattern spectra are used to compute probability size distribution functions of both protrusions and intrusions that are conspicuous in topography, based on which shape-size complexity measures of these sub-basins are estimated by means of average roughness and size. Furthermore, fractal dimensions of channel networks derived from these 14 basins are computed by applying the box-counting method. Comparisons between shape-size complexity measures and fractal dimension are carried out.

1. Introduction and motivation

Toward characterization of terrain from the point of its morphologic complexity, processing of digital elevation models (DEMs) derived from remotely sensed data has received notable attention. With the advent of interferometry techniques, it is possible to generate high spatial resolution DEMs with excellent accuracy (Graham 1974, Zebker and Goldstein 1986). DEM data are analysed in order to understand several characteristics of geoscientific interest in spatio-temporal mode (e.g. Turcotte 1997, Montgomery 2001, Stark and Stark 2001, Sagar and Tien 2004, Tay *et al.* 2005). These interests lie primarily in the fields of hydrology, geomorphology, geology, geophysics, ecology and environment.

With powerful computers and high-resolution DEMs, complex surficial characteristics of terrain can be analysed by using advanced mathematical concepts. Most terrain characterization techniques are mainly feature based and emphasize the spatial organization of specific features, that are essentially decomposed from terrain models or topographic maps, such as surface water bodies, unique connectivity networks (Sagar *et al.* 2003), watershed basins, mountain objects etc. Morphometry, fractal and allometric scaling analyses of these features provide various characteristics in a quantitative manner. Conventional morphometry-based network quantities are

*Corresponding author. Email: lttay@mmu.edu.my

International Journal of Remote Sensing
ISSN 0143-1161 print/ISSN 1366-5901 online © 2007 Taylor & Francis
http://www.tandf.co.uk/journals
DOI: 10.1080/01431160600981558

proposed by Horton (1945), and further significantly substantiated by Langbein (1947) and Strahler (1957). These topological quantities have been considered as the bases to compute scaling dimensions of basins and networks (e.g. Turcotte 1997, Rodriguez-Iturbe and Rinaldo 1997, Sagar and Tien 2004).

Roughness indexes have been shown to be informative tools for terrain analyses. The roughness of terrain reflects numerous geophysical parameters (e.g. basin characteristics, distributions of crenulations and degree of erosivity) and is useful for understanding basin-wise geomorphic process associated with exogenic processes. Earlier works on characterization of terrain through estimation of roughness indexes were done for geological and geomorphologic research (Strahler 1964, Stone and Dugundji 1965, Daniels *et al.* 1970, Franklin 1987, Nikora 2005). Other roughness measures that have been used include sigma-t (Ackeret 1990), 'roughness index' (Fatale *et al.* 1994) and fractal dimension (Goodchild 1980, Cherbit 1991). Most of the Earth's scale invariant topography and bathymetry are best modelled using fractal statistics (Turcotte 1997). Many researchers have carried out spectral analyses of topography (e.g. Gilbert 1989, Dubuc *et. al.* 1989, Turcotte 1997). Despite the monumental significance and usefulness of the spectral and fractal analyses for topographic description, it has little to offer in quantifying the shape and size content of topography possessing geometrical structure. Hence, quantitative analysis of surficial roughness has proven difficult because of its morphological complexity. Mathematical morphology (Matheron 1975, Serra 1982) is unquestionably one of the best approaches to quantify the shape and size content of basin-wise topography. In our earlier work (Tay *et al.* 2005), a simple framework based on mathematical morphological transformations is proposed to compute the complexity measures of DEMs. In the current paper, we show application of this morphology-based granulometric framework in deriving basin-wise terrain characteristics through shape-size complexity measures for Cameron Highlands and Petaling sub-basins. DEMs are delineated into meaningful basin-units of different shapes with varied degrees of complexities in their spatial forms. Furthermore, additional roughness index owing to both protrusions and intrusions of terrain is also derived and comparisons are carried out with fractal dimensions of the networks computed through the box-counting approach.

2. Methodology

2.1 *Basic definitions and notations of mathematical morphology*

DEMs are represented by function, f, where $f(x,y)$ (e.g. figure 1) is a function on Z^2 and B [figure 1(f)] is a structuring element (SE) of primitive size. The erosion (dilation) of f by B replaces the value of f at a pixel (x, y) with the minima (maxima) of the values of f over a structuring template B. We represent these grey level morphological transformations as

$$(f \ominus B)(x, y) = \min_{(i, j) \in B} \{f(x+i, y+j)\} \tag{1}$$

$$(f \oplus B)(x, y) = \max_{(i, j) \in B} \{f(x-i, y-j)\} \tag{2}$$

where $\ominus$ and $\oplus$ denote symbols for erosion and dilation respectively. The grey scale erosion and dilation transformations are illustrated in figures 1(a) and (b).

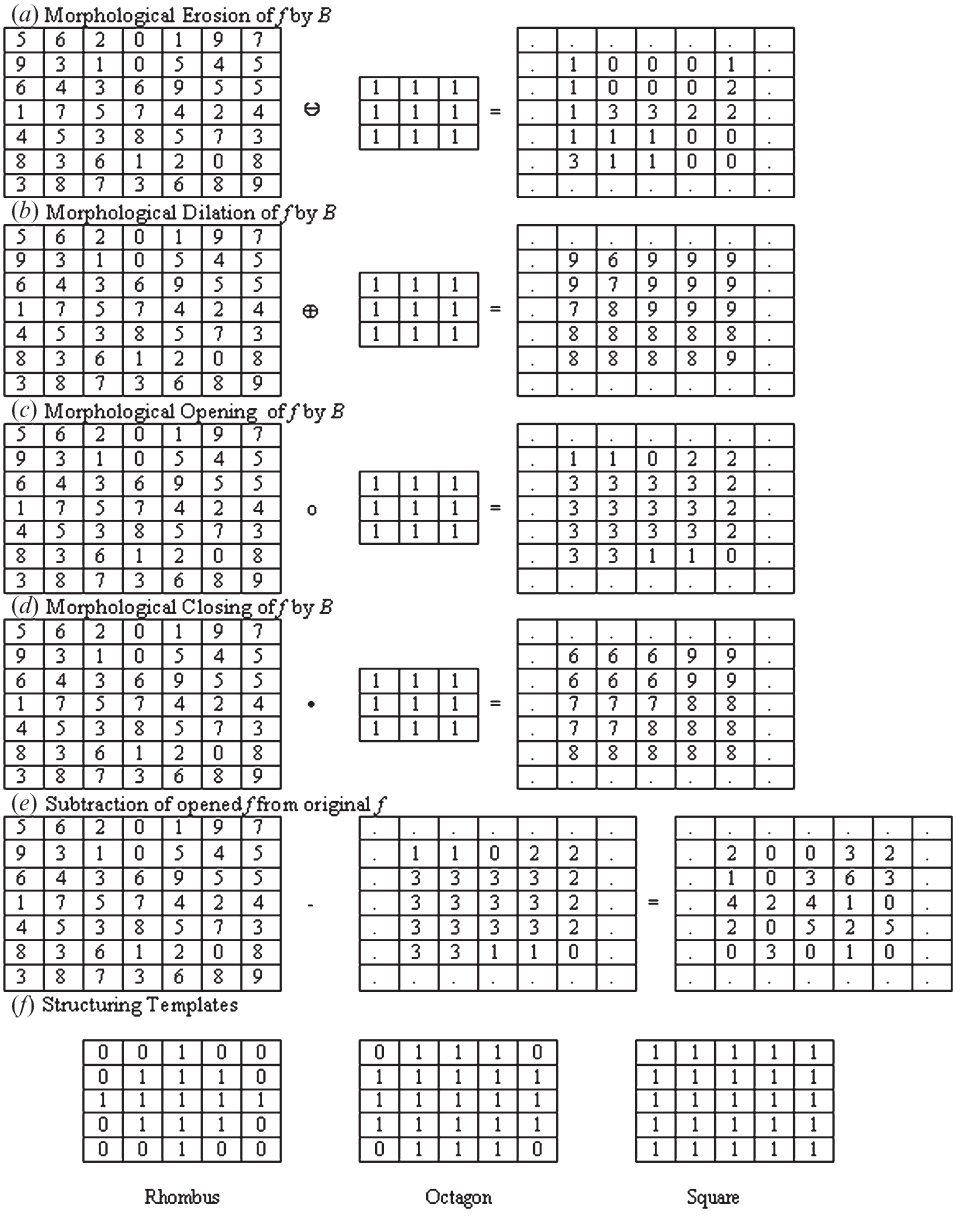

Figure 1. Greyscale morphological and logical transformations. (*a*) Erosion, (*b*) dilation, (*c*) opening, (*d*) closing, (*e*) subtraction of opened image from original image and (*f*) structuring templates required to generate multiscale effect. For this example DEM, area $A(f) = \sum_{(x,y)} f(x,y) = 0\ 232$, and $A[(f \circ B_0) - (f \circ B_1)] = 0\ 49$.

The grey level opening ($f \circ B$) and closing ($f \bullet B$) are cascades of erosion and dilation processes, as shown in equations (3) and (4) below

$$(f \circ B) = [(f \ominus B) \oplus B] \tag{3}$$

$$(f \bullet B) = [(f \oplus B) \ominus B] \tag{4}$$

These two operations are shown in figures 1(*c*) and (*d*).

Subsequently, multiscale opening ($f \circ B_n$) and closing ($f \bullet B_n$) can be performed by increasing the size (scale) of the structuring template B_n, where $n=0, 1, 2,\ldots, N$. These multiscale opening and closing of f by B are represented respectively as

$$(f \circ B_n) = \{[(f \ominus B) \ominus B \ominus \ldots \ominus B] \oplus B \oplus B \oplus \ldots \oplus B\} = [(f \ominus B_n) \oplus B_n] \tag{5}$$

$$(f \bullet B_n) = \{[(f \oplus B) \oplus B \oplus \ldots \oplus B] \ominus B \ominus B \ominus \ldots \ominus B\} = [(f \oplus B_n) \ominus B_n] \tag{6}$$

at scale $n=0, 1, 2,\ldots, N$.

Performing opening and closing iteratively by increasing the size of B transforms the DEM into lower resolutions correspondingly. Multiscale opening and closing of DEM by B_n effect spatially distributed elevation regions in the form of smoothing of contours to various degrees. The scale refers to size of SE. The bigger the SE, the larger the scale. The larger the scale, the more is the information loss from DEM, and hence the images possess lower resolution at the higher degree of scaling. The shape and size of B control the shape of smoothing and the scale respectively. These basic notations and transformations can be better understood by referring to figure 1.

2.2 *Granulometry*

Both protrusions and intrusions are computed using granulometry approach. The protrusions, information is derived by subtracting each opened version from the preceding level of opened version [equation (7)]. On the other hand, intrusions, information is obtained by subtracting the closed version from its succeeding level [equation (8)]. This information is named as the pattern spectra (Maragos 1989) of f relative to B for different size n

$$PS_f(+n, B) = A[(f \circ B_n) - (f \circ B_{n+1})],\ 0 \leq n \leq N \tag{7}$$

$$PS_f(-n, B) = A[(f \bullet B_n) - (f \bullet B_{n-1})],\ 1 \leq n \leq K \tag{8}$$

where $PS_f(+n,\ B)$ and $PS_f(-n,\ B)$ are the pattern spectra of foreground and background portions of f relative to B respectively, and $a(x)$–$b(x)$ is the point-wise algebraic difference between the two functions $a(x)$ and $b(x)$ [e.g. figure 1(*e*)].

The difference between the area of nth level opened basin and the area of $n+1$th level opened basin (where n ranges from 0 to N) is divided by the area of the original basin, $A(f)$ to get the probability function at nth level, $ps(n, f)$. In the same way, the difference between the area of nth level closed basin and the area of $n-1$th level closed basin (where n ranges from 1 to K) is divided by $A(f \bullet B_K)$–$A(f \bullet B_0)$ to get the probability function at nth level, $ps(-n, f)$. This descriptive procedure is mathematically expressed as

$$ps(n, f) = \frac{A(f \circ B_n) - A(f \circ B_{n+1})}{A(f \circ B_0)},\ n = 0, 1, 2, \ldots, N \tag{9}$$

where $0 \leqslant ps(n, f) \leqslant 1$.

$$ps(-n, f) = \frac{A(f \bullet B_n) - A(f \bullet B_{n-1})}{A(f \bullet B_K) - A(f \bullet B_0)},\ n = 1, 2, \ldots, K \tag{10}$$

where $0 \leqslant ps(-n, f) \leqslant 1$.

The probability function is the ratio between the area of the region that is obtained from algebraic difference between contiguous levels of opened (closed) basin and the total foreground (background) area of basin. These filtered features of f are a variety of crenulations that protrude above or intrude below f. A larger value of $ps(n, f)$ (or $ps(-n, f)$) infers that a larger amount of features protrude above (or intrude below) f.

Based on the probability size distribution functions of these distributed protrusions and intrusions, average size ($AS(f/B)$) and average roughness ($H(f/B)$) of foreground are estimated by incorporating probability function relative to B as follows

$$AS(f/B) = \sum_{n=0}^{N} nps(n, f) \tag{11}$$

$$H(f/B) = -\sum_{n=0}^{N} ps(n, f) \log ps(n, f) \tag{12}$$

To compute similar measures of background of f, we consider $ps(-n, f)$ of background portions of f estimated based on equation (10). To estimate the average roughness of basin owing to both foreground and background components, we employ the following equation:

$$H(f/B) = -\sum_{n=-K}^{n} \left[PS_f(n, B)/A(f \bullet KB)\right] \log\left[PS_f(n, B)/A(f \bullet KB)\right] \tag{13}$$

2.3 *Fractal analysis*

One of the important parameters used in fractal analysis is the fractal dimension (Feder 1988), which is also a widespread indicator of surface roughness. Fractal dimensions describe the space-filling property of the foreground objects in the image and it can be estimated through the box-counting method. The two-dimensional plane of the image is partitioned with a grid of squares of size r. The number $N(r)$ of square-grids that are traversed by foreground objects is counted. Using these parameters, fractal dimension of the foreground objects is computed as

$$D = \lim_{r \to 0} \frac{logN}{log(1/r)}$$

It is implemented by changing the value of r, and computing the corresponding N values. Estimation of the fractal dimension, D is done through the linear approximation of points (log N, log(1/r)) and this corresponds to the best-fit slope of the plot of log N versus log(1/r).

3. Study region DEMs and sub-watersheds

We employed intereferometrically derived topographic synthetic aperture radar (TOPSAR) DEM of Cameron Highlands region situated between 101°15′–101°20′ E. longitudes and 4°31′–4°36′ N. latitudes, and the Petaling region situated between 101°37′30″–101°40′ E. longitudes and 2°59′30″–3°02′ N. latitudes of Malaysia (figure 2) for terrain feature characterization. Cameron Highlands region is located in the eastern part of Perak state in Peninsular Malaysia. The physical relief of this area is rough where it comprises a series of mountainous forest at altitudes between 400 m and 1800 m. The Petaling region is located in the southern part of Selangor state in Peninsular Malaysia. This region is a relatively flat terrain with highest altitude of 215 m. Cameron Highlands DEM encompasses an area of 900×900 pixels with resolution of 10 m while Petaling DEM encompasses an area of 750×800 pixels with resolution 5 m. Figures 3 (*a*) and (*b*) show their three-dimensional shaded relief images. The height accuracy of TOPSAR DEMs has been shown to be 1 m root mean square (rms) in flat areas, 3 m rms in the mountain areas and 2 m rms overall (Madsen *et. al.* 1995). Based on the extracted channel networks, seven sub-basins are demarcated from Cameron Highlands DEM [figure 3(*c*)], and seven from Petaling DEM [figure 3(*d*)]. Figures 3(*e*) and (*f*) show the extracted channel networks of Cameron Highlands and Petaling regions respectively. The Cameron sub-basins are high altitude basins, whereas the sub-basins of Petaling belong to a relatively lower altitude region. The elevation ranges of Cameron basins are significantly higher than that of Petaling basins (table 1). All these 14 basins belong to two different major basins of these two physiographically distinct regions. Before initiating granulometry analysis, the networks and sub-basins extracted from the DEMs are analysed and compared with the topographic map. The extracted

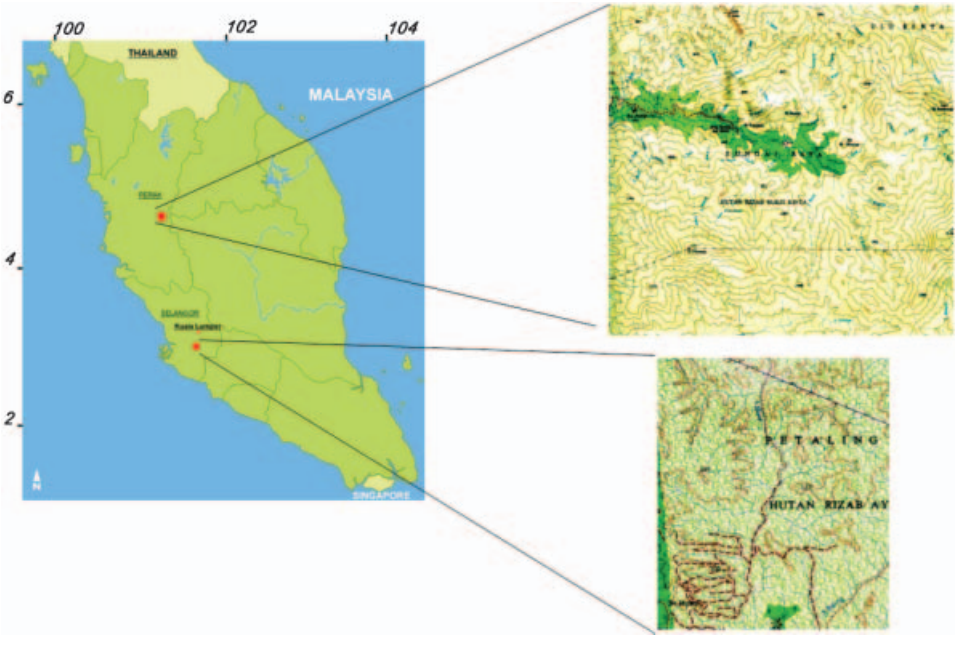

Figure 2. Location maps of Cameron Highlands and the Petaling region of Malaysia.

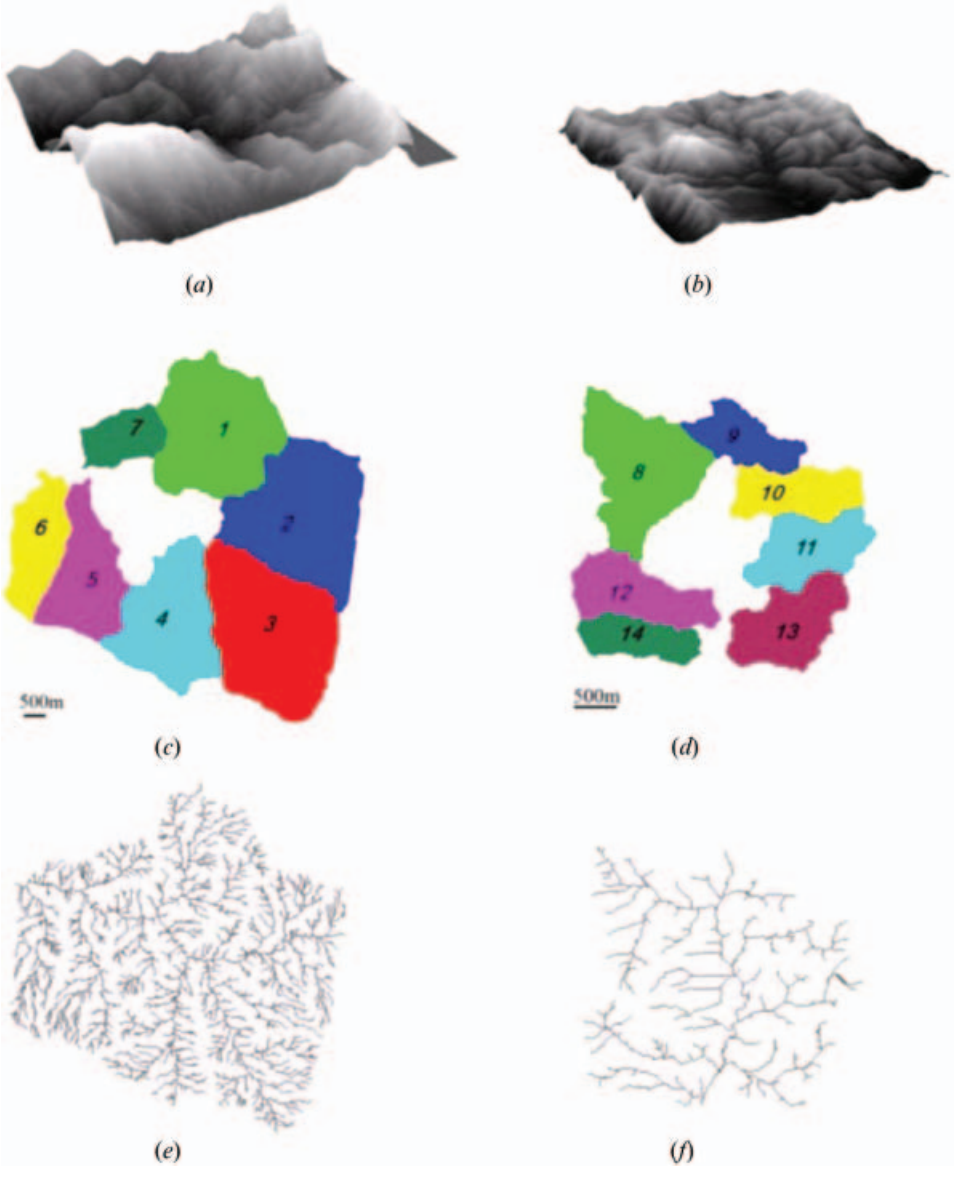

Figure 3. (*a*) Three-dimensional shaded relief image of TOPSAR DEM of Cameron Highlands, Malaysia; (*b*) three-dimensional shaded relief image of TOPSAR DEM of Petaling, Malaysia; (*c*) seven delineated sub-basins in different colours of Cameron Highlands DEM; (*d*) seven delineated sub-basins in different colours of Petaling DEM; (*e*) and (*f*) stream networks extracted from Cameron Highlands and Petaling DEMs, respectively.

networks from the DEMs are structurally synchronizing with that of topographic maps.

For these 14 sub-basins in both DEMs, we compute the shape-size complexity measures via granulometries, and compared these values with fractal dimensions of basin-wise networks computed through the box-counting method (Feder 1988). Figure 4 shows a flowchart depicting the step-wise procedures followed in this

Table 1. Basic measures of basin size, height and maximum number of iteration for all 14 basins.

Basin number N	Basin size (No. of pixels)	DEM height				Maximum number of iteration		
		Max (m)	Min (m)	Max–min (m)	Relief ratio	Square	Octagon	Rhombus
1	105400	1280.1	540.6	739.5	0.422	170	227	340
2	137463	1596.5	591.8	1004.7	0.371	208	277	415
3	131517	1695.9	587.4	1108.5	0.346	214	285	427
4	107625	1594.5	570.5	1024.0	0.358	188	250	375
5	89300	1745.2	503.0	1242.2	0.288	190	254	380
6	60520	1667.7	483.4	1184.3	0.290	178	238	356
7	36814	929.6	475.9	453.7	0.512	117	156	233
8	134400	208.0	54.3	153.7	0.261	210	280	420
9	57950	155.7	50.7	105.0	0.325	153	204	305
10	48000	193.5	48.7	144.8	0.251	160	214	320
11	68800	192.7	40.7	152.0	0.211	160	214	320
12	72000	215.7	32.9	182.8	0.152	180	240	360
13	72500	153.2	31.7	121.5	0.207	145	194	290
14	42000	169.1	27.6	141.5	0.163	150	200	300

investigation. Table 1 provides the basic measures for the 14 decomposed basins such as basin areas, maximum and minimum elevation heights in metres, elevation ranges, relief ratio and maximum number of iterations needed for multiscaling with respect to square, octagon and rhombus structuring elements. We calculate the maximum number of iteration, *N*max based on the size of the basin and shape of the structuring element. For a basin of size X columns × Y rows, the maximum possible size of structuring element (square) is $2 \times X$ if X is greater than Y or $2 \times Y$ if Y is greater than X. The maximum possible iteration, *N*max is then derived from the maximum size of structuring element.

Local foreground and background in the DEM represent higher and lower local elevations respectively. Granulometries by opening and closing of DEM generate DEMs at multiple scales, where various sizes of protrusions and intrusions from foreground and background structures are filtered out respectively. We perform multiscale opening and closing on sub-basins of Cameron Highlands and Petaling by means of symmetric square, octagon and rhombus templates [figure 1(*f*)]. The three symmetric templates used are referred as SEs, which play an important role in the granulometric analysis. Illustrations of specific resultant multiscale basin at multiple scales can be seen in figure 5. We observe a large flat plateau [figure 5(*a*)–(*c*)] and flat sinks [figure 5(*d*)–(*f*)] shaped like B_n at large scales n of the opening ($f \circ B_n$) and the closing ($f \bullet B_n$), respectively.

We compute basin-wise areas of protrusions and intrusions, from Cameron Highlands and Petaling sub-basins, that are filtered out at respective scales to estimate the probability functions [equations (9) and (10)]. By incorporating these probability functions computed for each basin by means of three different morphological structure rules, we estimated the shape-size complexity measures (average sizes and average roughness) for both foreground and background of all 14 sub-basins. These shape-size complexity measures show apparent discrimination among the 14 sub-basins. These scale independent measures rely on topologic

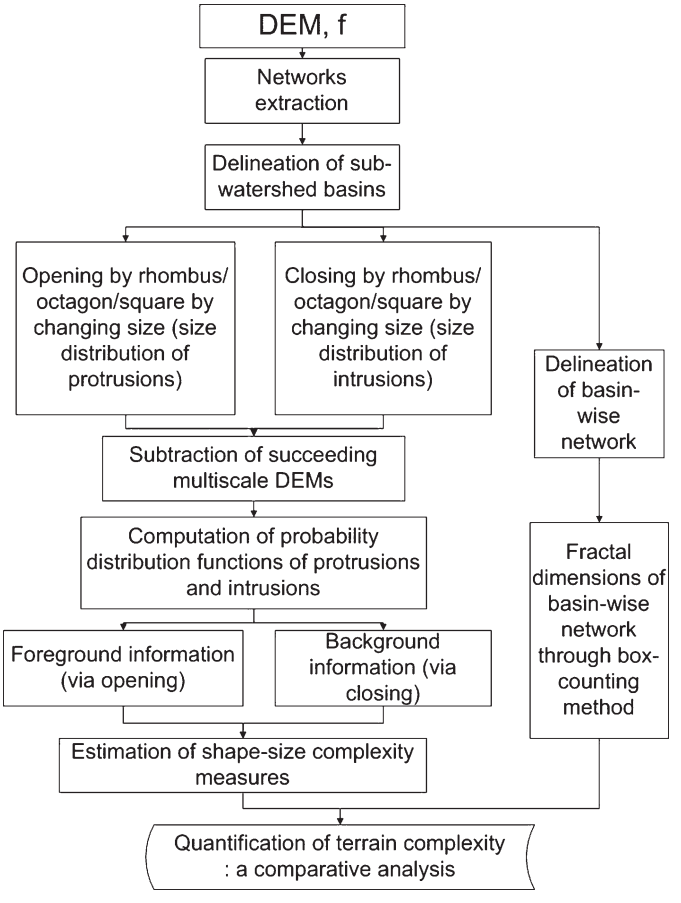

Figure 4. Flowchart depicting the sequential steps adapted in this investigation.

and geometric criteria and they can be considered as the indicators to understand the complexity of surface owing to size distributions of its protrusions/intrusions.

Average roughness quantifies the shape-size complexity of f by means of its surface roughness due to their protrusion and intrusion distribution averaged over all depths that B reaches. We normalize average roughness index with $\log(N\max)$ so that the normalized index is in the range of zero to one, where $N\max$ is the maximum possible iteration needed for morphological opening (closing) to convert the basin image to become totally black (white) or minimum (maximum) (table 1). If both intrusions and protrusions are considered, overall roughness index is derived using equation (13) with respect to the three structuring elements. The overall roughness index is normalized with $\log(2 \times N\max)$. Figure 6 illustrates the average size and normalized average roughness of the foreground and background for the 14 sub-basins whereas the overall roughness indexes are shown in figure 7.

In order to obtain the fractal dimension for the 14 sub-basins, the channel networks for the DEM are extracted [e.g. figures 3(e) and (f)]. Fractal dimensions of these networks are computed by using the box-counting method where extracted

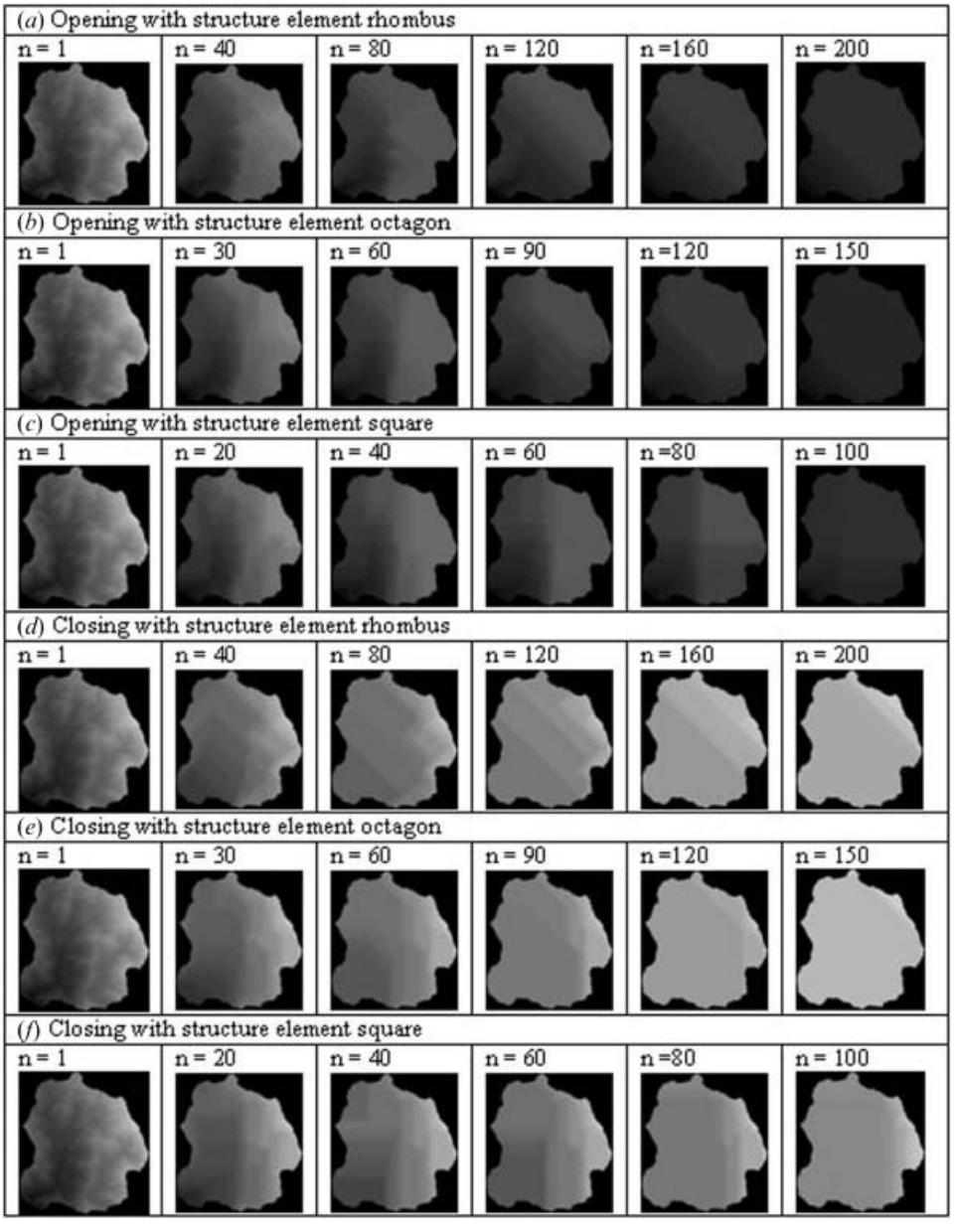

Figure 5. Basin 1 of Cameron Highlands is taken as an example to show the basin images at multiple scales generated via closing and opening. Basin 1 is located at the northern part of Cameron Highlands region, with a size of 3.1 km (east to west) × 3.4 km (north to south). (*a–c*) DEM at multiple scales generated via opening by means of rhombus, octagon, and square, respectively; (*d–f*) multiscale DEMs generated via closing by means of rhombus, octagon, and square, respectively.

networks of both DEMs are considered as foreground objects. The number N(r) of square-grids (size r) that are traversed by network elements is counted. Fractal dimensions of the networks of these 14 sub-basins are computed through the linear

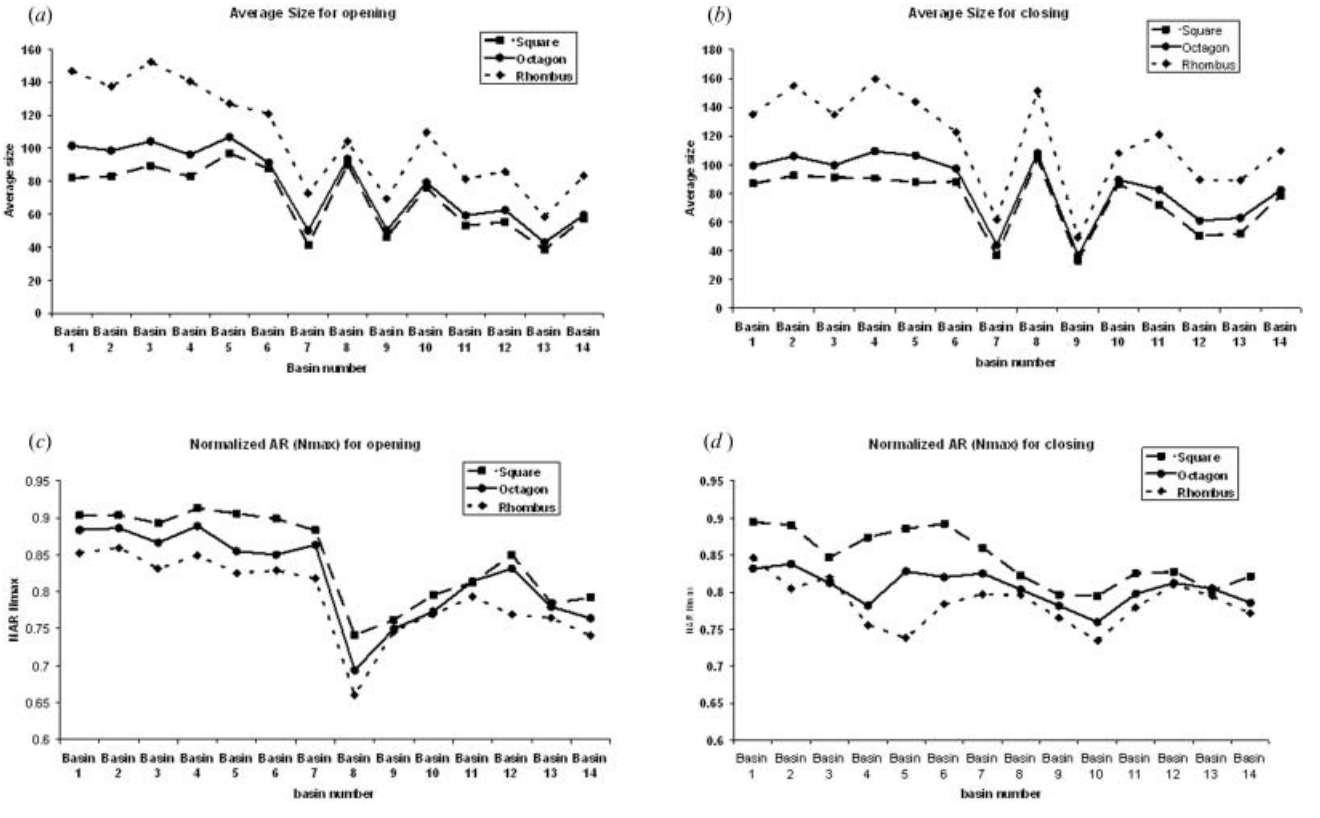

Figure 6. Mean size and roughness values vs basin number. (*a–b*) average size values computed, for foregrounds and backgrounds of 14 basins by means of square, octagon and rhombus, and (*c–d*) normalized mean roughness values computed for foregrounds and backgrounds of fourteen basins by means of square, octagon and rhombus.

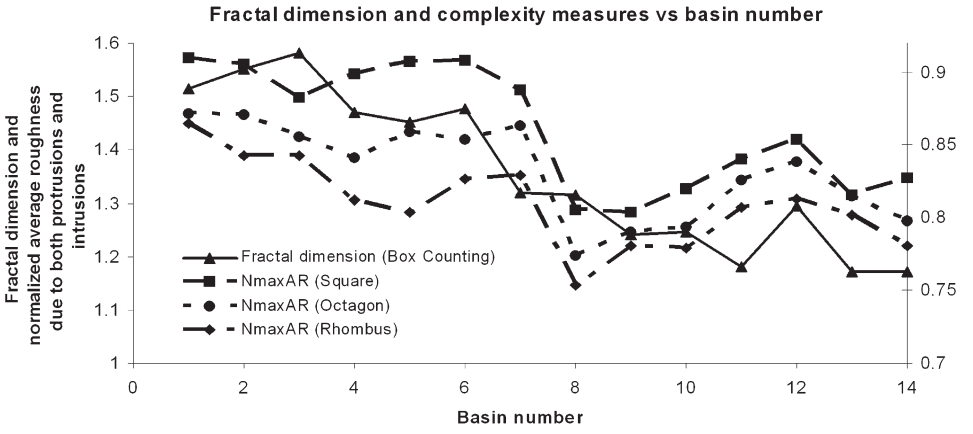

Figure 7. Fractal dimensions and overall roughness measures versus basin number.

Table 2. Fractal dimensions for the 14 sub-basins.

Basin	Fractal dimension (via box counting)
1	1.5141
2	1.5506
3	1.5814
4	1.4692
5	1.4519
6	1.4776
7	1.3192
8	1.3140
9	1.2398
10	1.2445
11	1.1817
12	1.2946
13	1.1706
14	1.1721

approximation of graph (log N, log(1/r). This estimation corresponds to the best-fit slope of the plot (log N versus log(1/r). The best-fit fractal dimensions for the networks extracted from these basins are given in table 2 and figure 7. The fractal dimension values explain the space-filling characteristics of networks. The higher the dimension, the higher is the network density or space-filling property, and *vice versa*.

4. Results and discussion

The considered three primitive templates [figure 1(*f*)] used to perform granulometric analysis are square (25 elements), octagon (21 elements) and rhombus (13 elements) in the order of decreasing number of elements. Iterative openings and closings are performed by means of these three templates on 14 basins until the basins become completely dark (grey value 0) and completely bright (grey value 255) respectively.

The number of iterations required to make each sub-basin either become darker or brighter depends on the size, shape, origin, orientation of considered primitive template to perform multiscale openings or closings, and also on the size of the basin and its physiographic composition. More opening/closing cycles are needed when structure element rhombus is used, and it is followed by octagon and square.

It is obvious from figures 6(*a*) and (*b*) that mean size values of foreground and background regions of DEM computed for these sub-basins are highest when rhombus structuring element is used, and it is followed by octagon and square. Generally, mean size values depend on the total size of protrusions and intrusions filtered via granulometric analyses. Estimated average sizes of protrusions (intrusions) are also dependent on the probing rule. For instance, the larger average size values of protrusions are obtained for basins 1, 2, 3 and 4, and intrusions for basins 2, 4, 5 and 8 by means of rhombus template. These average size values by means of octagonal and square-type rules have not followed exactly the trend like the values computed by means of rhombus. Hence, average size of the basin, which is scale independent, is shape dependent.

On the other hand, mean roughness indicates the shape-content of the basins. Higher mean roughness for a basin with respect to a particular structuring element indicates higher value of surface roughness within the basin boundary, relative to that structuring element. The average roughness values in normalized scale are computed by considering the ratio between average roughness values [equation (12)] and the *N*max (table 1) in logarithm scale. A clear distinction is obvious between the Cameron and Petaling basins [figure 6(*c*)]. Generally, roughness values of Cameron basins are significantly higher than that of Petaling basins. The ranges of normalized roughness values for foreground (background) by means of square are 0.88–0.91 (0.84–0.89) for Cameron basins and 0.74–0.85 (0.79–0.83) for Petaling basins. These ranges are significantly different from that of octagon and rhombus. Relatively, Petaling basins possessing lower normalized average roughness values than that of Cameron highlands basins. All Petaling basins, of which the normalized average roughness values ranging from 0.66–0.85 (foreground) and 0.73–0.83 (background) depict the basins are relatively more smooth than that of Cameron basins with roughness values of 0.81–0.91 (foreground) and 0.73–0.89 (background) for all three structuring elements used. The overall roughness indexes (owing to both protrusions and intrusions) estimated with respect to square for the seven Cameron basins range between 0.89 and 0.91 clearly depicting the distinction with Selangor basins, for which these values range between 0.80 and 0.85 (figure 7). All the Cameron basins, being high altitude basins, possess greater relief differences than Petaling basins (table 1). It has been shown that a change in the characteristic information of the probing template shows different shape–size complexity measures. Influences of structuring elements on each basin depend on the shape of the SE. As long as the shape of SE is geometrically similar to basin regions, the average roughness result possesses lower analytical values. If the topography of basin is very different from the shape of SE, high roughness results are produced which indicate that the basin is rough relative to that SE. In general, all basins are more rugged relative to square shape as highest roughness index are derived when square is used as SE.

The unique networks that reflect the general characteristics of surface morphology, are characterized via fractal concepts. The fractal dimensions of the basin-wise channel networks extracted from DEMs also show clear distinction between

these two regions (table 2). Relatively, Petaling sub-basins have a sparser network as compared with the intricate networks of Cameron highlands sub-basins. These complexities are better reflected from the fractal dimension values that range from 1.31–1.58 for Cameron basins, and 1.17 – 1.31 for Petaling basins. These observations are supporting to infer those Petaling basins, being low lying basins, possess different geomorphic set up while comparing with that of Cameron basins, which are higher altitude basins. Fractal dimensions of the abstract structures of concave zones that are conspicuous in DEMs have not followed exactly the similar trends of any of the three roughness values (derived using three different SEs), which are shape dependent. Specifically, higher fractal dimension value of the network indicates higher space-filling characteristics of the networks.

Significant differences between the values for two distinct physiographic regions, derived via granulometric analysis of foreground and background regions and fractal analysis of networks of basins, are observed. These significant variations are due to the physiographic, geomorphic, geophysical and geologic distinctions. The terrain complexity measures derived granulometrically are scale-independent, but strictly shape-dependent as evident from figure 6. In geomorphology, many processes are linked with geometric, topologic, and morphologic organization of the system. The shape-dependent complexity measures that are sensitive to record the variations in basin shape, topology, and geometric organization of hillslopes provide potentially valuable insights as compared to that of fractal dimension values. This framework further facilitates the process of classifying the watersheds based on these geometrically and topologically significant shape-size based measures.

5. Conclusions

Two popular methods, namely granulometry (frequency of distribution of protrusions and intrusions), and fractal analysis of networks are employed to characterize basin-wise morphology. The basic difference between these two methods lies in the media employed. Derivations of granulometry-based complexity measures are based on sub-watersheds in a spatially distributed elevation model, where the basins are considered as discrete sub-functions at multiple scales that are simulated via opening and closing transformations. On the other hand, fractal dimension of the geophysical channel network represented in binary form is derived through the box counting method. Both granulometry and fractal techniques are tested on sub-basins of various sizes and shapes decomposed from DEMs of two distinct geomorphic regions. Granulometry-based measures provide shape–size-based content, unlike spectral content that is usually computed based on Fourier spectral analysis. These complexity measures are unique, and scale invariant. Terrain classification can be implemented using these measures and fractal dimension for lower-order sub-basins that are hierarchically decomposed from higher-order basins. The granulometry-based basin-wise measures have more practical applications due to the shape-dependent property, which has more direct implications to explore possible links with the geomorphic processes involved. Future works on the derivation of direction-specific roughness values is possible with the use of specific SE and topographic signatures in certain direction. Besides, open problems in exploring the links between these basin-wise values and field based results are potential future works.

Acknowledgements

We gratefully acknowledge the Malaysian Centre for Remote Sensing (MACRES) for providing Cameron Highlands and Petaling DEM data. We are grateful to the Editor for the invaluable comments and suggestions provided.

References

ACKERET, J.R., 1990, Digital terrain elevation data resolution and requirements study. Interim report ETL-SR-6, U.S. Army Corps of Engineers.

CHERBIT, G., 1991, *Fractals Non-integral Dimensions and Applications* (Chichester: John Willey).

DANIELS, R.B., NELSON, L.A. and GAMBLE, E.E., 1970, A method of characterizing nearly level surfaces. *Zeitscheift fur Geomorphologies*, **14**, pp. 175–185.

DUBUC, B., ZUCKER, S.W., TRICOT, C., QUINIOU, J.F. and WEHBI, D., 1989, Evaluating the fractal dimension of surface. *Proceedings of the Royal Society of London*, **A425**, pp. 113–127.

FATALE, L., ACKERET, J.R. and MESSMORE, J., 1994, Impact of digital terrain elevation data (DTED) resolution on army applications: simulation vs. reality. *Proceeding American Congress on Surveying and Mapping American Society for Photogrammetry and Remote Sensing*, **2**, pp. 89–104.

FEDER, J., 1988, *Fractals* (New York, NY: Plenum Press).

FRANKLIN, S., 1987, Geomorphometric processing of digital elevation models. *Computers and Geosciences*, **13**, pp. 603–609.

GILBERT, L.E., 1989, Are topographic data sets fractal? *Pure and Applied Geophysics*, **131**, pp. 241–254.

GOODCHILD, M.F., 1980, Fractals and accuracy of geographical measures. *Mathematical Geology*, **12**, pp. 85–98.

GRAHAM, L.C., 1974, Synthetic interferometer radar for topographic mapping. *Proceedings of the IEEE*, **62**, pp. 763–768.

HORTON, R.E., 1945, Erosional development of stream and their drainage basin: hydrological approach to quantitative morphology. *Bulletin of the Geophysical Society of America*, **56**, pp. 275–370.

LANGBEIN, W.B., 1947, Topographic characteristics of drainage basins. *U.S. Geological Survey Professional Paper*, **968-C**, pp. 125–157.

MADSEN, S.N., MARTIN, J.M. and ZEBKER, H.A., 1995, Analysis and evaluation of the NASA/JPL TOPSAR Across-Tack Interferometric SAR System. *IEEE Transactions on Geoscience and Remote Sensing*, **33**, pp. 383–391.

MARAGOS, P.A., 1989, Pattern spectrum and shape representation. *IEEE Transactions Pattern Analysis and Machine Intelligence*, **11**, pp. 701–716.

MATHERON, G., 1975, *Random Sets and Integral Geometry* (Hoboekn, New Jersey: John Wiley).

MONTGOMERY, D.R., 2001, Slope distributions, threshold hillslopes, and steady-state topography. *American Journal of Science*, **301**, pp. 432–454.

NIKORA, V.I., 2005, High-order structure functions for planet surfaces: a turbulence metaphor. *IEEE Geoscience and Remote Sensing Letters*, **2**, pp. 362–365.

RODRIGUEZ-ITURBE, I. and RINALDO, A., 1997, *Fractal River Basins: Chance and Self-organization* (Cambridge: Cambridge University Press).

SAGAR, B.S.D. and TIEN, T.L., 2004, Allometric power-law relationships of Hortonian Fractal digital elevation model. *Geophyiscal Research Letters*, **31**, pp. L06501.

SAGAR, B.S.D., MURTHY, M.B.R., RAO, C.B. and RAJ, B., 2003, Morphological approach to extract ridge-valley connectivity networks from digital elevation models (DEMs). *International Journal of Remote Sensing*, **24**, pp. 573–581.

SERRA, J., 1982, *Image Analysis and Mathematical Morphology* (London: Academic Press).

STARK, C.P. and STARK, G.J., 2001, A channelization model of landscape evolution. *American Journal of Science*, **301**, pp. 486–512.

STONE, R. and DUGUNDJI, J., 1965, A study of microrelief- Its mapping, classification, and quantification by means of a Fourier analysis. *Engineering Geology*, **1**, pp. 89–187.

STRAHLER, A.N., 1964, Quantitative geomorphology of drainage basins and channel networks. In *Handbook of Applied Hydrology*, V.T. Chow, (Ed), pp. 4-39–4-76 (New York: McGraw-Hill).

TAY, L.T., SAGAR, B.S.D. and CHUAH, H.T., 2005, Derivation of terrain roughness indiactors via Granulometries. *International Journal of Remote Sensing*, **26**, pp. 3901–3910.

TURCOTTE, D.L., 1997, *Fractals in Geology and Geophysics* (Cambridge: Cambridge University Press).

ZEBKER, H.A. and GOLDSTEIN, R.M., 1986, Topographic mapping from interferometric Synthetic Aperture Radar observations. *Journal of Geophysical Research*, **91**, pp. 4993–4999.